

Influence of Si Addition on the Recrystallization Texture of Al-Mn-Mg Aluminum Alloy

CHUNG-YI YU*, JUNG-PANG CHANG**, SHI-XUAN DING*,
TIEN-YU TSENG* and HAN-CHENG SHIH*

**New Materials Research & Development Department
China Steel Corporation*

***Research & Development Department
China Steel Aluminum Corporation*

Al-Mn-Mg aluminum alloy ingots with different Si additions produced by DC (Direct-Chill) casting were used in this study. After homogenization, recrystallization texture evolution was investigated by proper combination of the thermomechanical process simulator (Gleeble 3800) and heat treatment. The result shows that the recrystallized grain growth rate is decelerated with increasing Si content. It could be attributed to that the more the amount of coherent dispersoids precipitated results in strengthening the retarding force on grain/subgrain boundaries upon growth. Additionally, the recrystallization texture exhibits an evidently dependence on the number of particles with a diameter larger than the critical value d_c . The number of these active particles, the potential incubation sites for Particle Stimulated Nucleation (PSN), increases with Si contents results in the weakening of the intensity of the Cube component. However, the phenomenon could be described quantitatively in terms of the criterion recommended by Humphreys, excluding the specimen with fraction recrystallized $< 85\%$.

Keywords: Si additions, Recrystallization, Texture, Cube component

1. INTRODUCTION

In order to survive in this competitive market of high energy, raw material costs, and relatively low finished goods prices, beverage can manufacturers exert every effort to minimize conversion costs while maximizing the recoverable metal units, ex the Used Beverage Can (UBC). The use of UBC can reduce the need for imports, and recycling also saves $\sim 95\%$ of both the energy and greenhouse gas emissions associated with the smelting of aluminum from the original bauxite ore⁽¹⁾. Due to the unique benefits in energy saving (economic) and environmental protection, the additional amount of UBC has increased dramatically in all aluminum mills. But a major drawback for the intensive use of UBC is the presence of impurity elements at unsuitable high levels, which results in the formation of detrimental ears on the cup rim after drawing⁽²⁻⁵⁾. These ears are protruded by an ironing process and have to be trimmed before the next processing. Hence, the material wastage will increase.

It is generally known that a minimum earing can be achieved by the counterbalance between the deformation and recrystallization textures⁽⁴⁻⁷⁾. One of the most important factors in controlling recrystallization

and texture is the second phase particle distribution of aluminum alloy. According to the literature reports⁽⁸⁻¹¹⁾, the coarse primary particles ($> 1\mu\text{m}$) act to promote nucleation of new recrystallized grains due to Particle Stimulated Nucleation (PSN), and cause a more randomized texture compared to that of a particle free alloy with the same deformation history. The smaller dispersoid particles have a retarding effect by pinning the grain/subgrain boundaries on the rate of recrystallization due to the zener pinning processes^(3,8-9). Therefore, the required final microstructure and texture for beverage can body making can be obtained by appropriate manipulation of the thermomechanical process to balance between the two types of particle (constituents and dispersoids)^(2-3,8).

Elemental Si of Al-Mn-Mg Aluminum alloy also has a significant influence on recrystallization behavior and texture evolution through the different kinds of particles^(2-3,12). More attention has been paid to the effects of intermetallics bearing Fe and Mn^(2,4-7), however, the understanding of the effects of Si content on the recrystallization and texture is still restricted. Consequently, the various Si contents were introduced into Al-Mn-Mg aluminum alloy by a proper combination of DC casting and homogenization treatment. After hot

deformation, the recrystallization kinetics as well as the texture evolution was investigated by means of heat treatment in this study. The solid solution effect of atom Si was evaluated in this study as well. In addition, the mechanism of texture evolution was analyzed quantitatively.

2. EXPERIMENTAL METHOD

Al-Mn-Mg aluminum alloy ingots with different Si additions in Table 1 were produced by laboratory DC casting in this study. Then, the ingots were homogenized at 600°C isothermally for 24h to minimize the alloy microsegregation phenomenon. In addition, the electrical conductivity measurement was used here for assessing the alterations of solid solution before and after homogenization.

Plain Strain Compression (PSC) specimens of 38 mm in length, 25 mm in width and 15 mm in thickness were machined from the homogenized material. The experiments were performed by a Gleeble-3800 thermomechanical process simulator to simulate the industrial hot tandem rolling. The specimens were uniaxial multi-compressed to a total true strain of 2.4 at 360°C under a constant strain rate of 50s⁻¹. A thermocouple was affixed at the middle of the specimen to measure the instantaneous temperature during compression. Lubricated with graphite at the anvil-platen/specimen interface, all specimens were heated to each deformation temperature at the rate of 5°C/s, and held for 90s prior to compression. After deformation, the specimens were quenched to ambient temperature to conserve the hot deformed microstructure. The specimens were then annealed in a salt bath at 340°C for various lengths of time and quenched so that the static recrystallization kinetics could be metallographically determined. Electron Backscattering Diffraction (EBSD) was used to quantify the percentage recrystallized in each specimen. EBSD mapping acquired by automatic scanning with steps (pixel size) of 2µm was carried out using a Field Emission Gun Scanning Electron Microscope (FEG-SEM) equipped with a HKL Channel 5 system.

The annealed specimens were mounted, polished, and anodized using Barker's reagent so that the microstructure evolution could be examined optically. In addition, the particle morphologies and distributions

before and after PSCed tests were observed by means of the FESEM. All microstructural characterizations were carried out in a FEI G2 Transmission Electron Microscope (TEM) operated at 120 kV. Its preparation method has been reported elsewhere, which will not be described here⁽¹³⁾.

The crystallographic texture measurement was measured on the compression plane by the use of X-ray diffractometer. Four incomplete pole figures, namely {111}, {200}, {220} and {311}, were measured at mid-thickness by the Schulz reflection method using Mo K α radiation⁽¹⁴⁾. Orientation Distribution Functions (ODFs, f(g)) were subsequently computed with series expansion method ($l_{\max}=22$) from the experimental pole figures⁽¹⁴⁾. The orientations are expressed in the form of a triple of Euler angles (ϕ_1, Φ, ϕ_2) according to Bunge's notation^(9,14).

3. RESULTS AND DISCUSSION

Typical morphology of the primary eutectic constituent particle of Al-Mn-Mg aluminum alloy before and after homogenization was observed by SEM, as shown in Fig.1. It shows that the script-like particle of the as-cast sample in Fig.1(a) has been spheroidized and transferred into smaller and discrete granules in Fig.1(b) after a homogenization treatment at 600°C for 24h. In addition, the constituent particle size decreases with increasing the Si concentrations (not shown here). Instantaneously, the dispersoid particles within grain interior also precipitate from the supersaturated matrix in Fig.1(b). Therefore, a bimodal distribution consisted of two kinds of particles can be obtained. It will exhibit an intense effect on the microstructural development, especially for the recrystallization behavior during subsequent processing.

In respect of the phase identification, the major phase of the as-cast Al-Mn-Mg aluminum alloy is the Al₆ (Fe, Mn). A lesser amount of Al₁₂ (Fe, Mn)₃Si, named α_c is present, and some Mg₂Si is usually observed. After homogenization, the constituent Al₆ (Fe, Mn) phase has transformed into α_c phase as shown in Fig.2. The peak intensity of the transformed α_c phase becomes stronger gradually with increasing the concentrations of Si. The similar tendency measured via the electrical conductivity is also listed in Table 2. The Si addition would like to stimulate the precipitation

Table 1 Main chemical compositions of Al-Mn-Mg aluminum alloys (wt%)

Sample	Si	Fe	Mn	Mg	Al
L-Si	0.09	0.39	1.30	1.20	Bal.
N-Si	0.23	0.38	1.31	1.20	Bal.
H-Si	0.42	0.38	1.29	1.21	Bal.

causing the amount of the solid solution to decrease. For H-Si specimen, the formation of the $Al_6(Fe, Mn)$ phase was suppressed, however, as the amount of Si to 0.09 wt%, the particle preferred to form the $Al_6(Fe, Mn)$ phase rather than to form the α_c phase. Obviously, the addition of Si has great influence on the phase formation and its particle size in Al-Mn-Mg aluminum alloy.

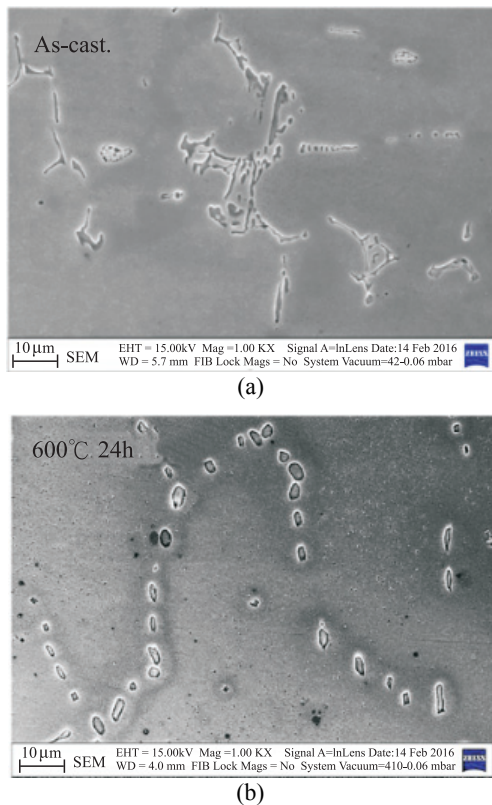


Fig.1. (a) Microstructure observations of the primary constituent particle of the Al-Mn-Mg aluminum alloy before, and (b) after homogenization.

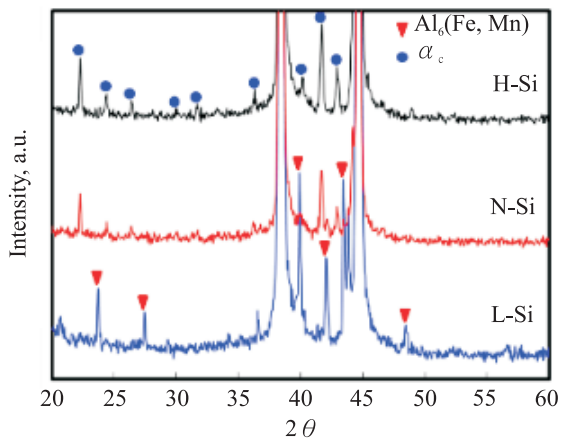


Fig.2. XRD patterns of the Al-Mn-Mg aluminum alloy after homogenization at 600 °C for 24h.

Table 2 Electrical conductivity of Al-Mn-Mg aluminum alloys before and after homogenization at 600 °C -24 hours

Sample	IACS%	
	Before	After
L-Si	29.2	35.8
N-Si	29.6	37.2
H-Si	28.6	39.8

Figure 3(a) is a typically as-PSCed microstructure observed via Polarization Optical Microscope (POM). It reveals a deformed structure with elongated grain morphology along the longitudinal direction. The microstructural evolution was observed through isothermal annealing at 340°C with different lengths of time as shown in Fig.3(b). In the first row (annealing time 180s), there was a little discrepancy among the samples except for the specimen H-Si which exhibits a larger grain size. With annealing time increased to 300s, the specimen L-Si has fully achieved-recrystallization, but the other two samples still retain lots of deformed structure in Fig.3. As the annealing time lengthened to over 600s, only the specimen H-Si exhibits the partial recrystallization.

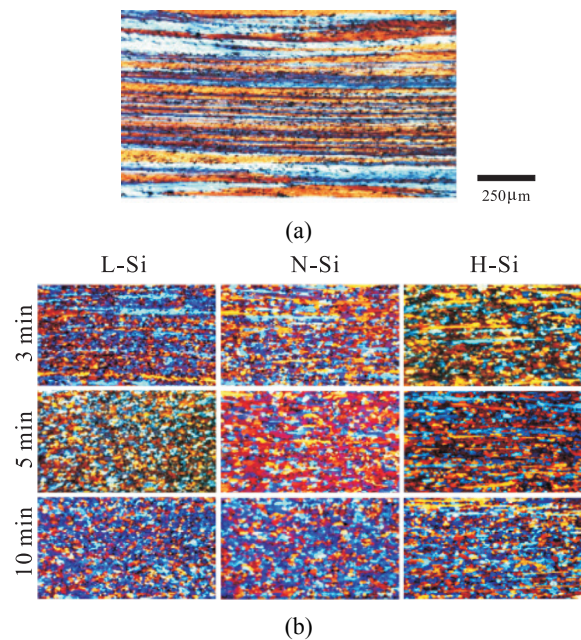


Fig.3. (a) Polarization optical micrograph of as PSCed specimen showing the typically elongated grain structure, and (b) the evolution of the microstructure with increasing annealing time.

The corresponding volume fraction recrystallized (X_v) was evaluated by the use of the EBSD. The dependence of Si contents upon recrystallization kinetics of Al-Mn-Mg aluminum alloy annealed at 340°C is shown in Fig.4. In the very beginnings, all conditions show a nearly incubated period. But the boundary mobility of the specimens having higher Si has been decelerated apparently with extending the annealing time. Additionally, the specimen L-Si owning the highest amount of the solid solution in Table 2 takes the least amount of time on average for fully achieving recrystallization instead. Hence, the retarding force of the solid solution seems to have little influence on the boundary migration.

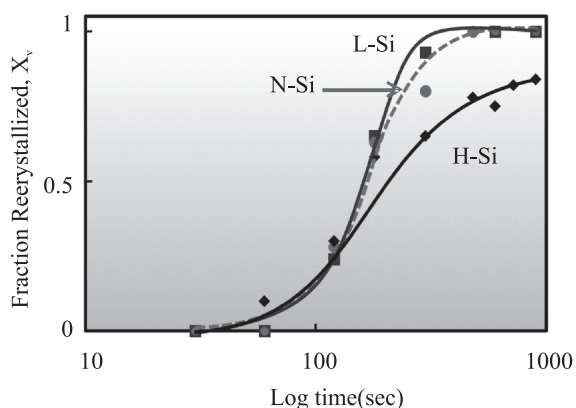


Fig.4. Effect of Si additions on the isothermal recrystallization kinetics of Al-Mn-Mg aluminum alloy.

Figure 5 is the dispersoid observations of Al-Mn-Mg aluminum alloys with different Si additions. It shows that a number of the dispersoids precipitate multiplicatively both in grain interior and at the boundary with increasing Si contents. The dispersoid could act as an obstacle to reduce boundary motion efficiently. There-

fore, the period from nucleation to fully recrystallization has been prolonged in Fig.4. As a result, the time for achieving fully recrystallization of the specimen N-Si falls behind the specimen L-Si. For the specimen contains the highest Si concentration, however, the migration of the recrystallized grain boundary has been impeded, particularly as the X_v value is over 50%. Even with modifying heat treatments via either raising temperature or prolonging the duration, the deformation structure still retains. The highest volume fraction recrystallized is no more than 85%.

In order to clarify the phenomenon, the particles Orientation Relationship (OR) was analyzed by means of TEM technology. The dispersoids of the specimens L-Si and N-Si have been characterized as incoherency as shown in Fig.6(a). And there were fewer coherent particles that could be discovered. On the other hand, the specimen H-Si has lots of coherent dispersoids, especially at grain boundary in Fig.5(b). The crystallographic OR of the coherent dispersoids in specimen H-Si has been determined to

$$[1\bar{1}1]_{\alpha c} // [1\bar{1}1]_{Al} ; (275)_{\alpha c} // (022)_{Al} ; (75\bar{2})_{\alpha c} // (\bar{2}20)_{Al}$$

as shown in Fig.6(b). The correlation between the pinning pressure of dispersoids and the migration rate of the recrystallized boundaries can be expressed in terms of the Zener drag force Z , which is expressed in^(4-5,8-9)

$$Z = k \frac{f_v \gamma_{gb}}{\bar{r}} \dots\dots\dots(1)$$

where f_v and \bar{r} are the volume fraction and the average radius of dispersoids, respectively, γ_{gb} is the interfacial energy of the grain boundary, and k is a constant related to coherency. In general, the k value of incoherent dispersoid is 3/2, but that of coherent dispersoid is about 6⁽¹⁵⁾. This suggests that coherent particles will be at least nine times more effective than incoherent particles in restraining grain boundary

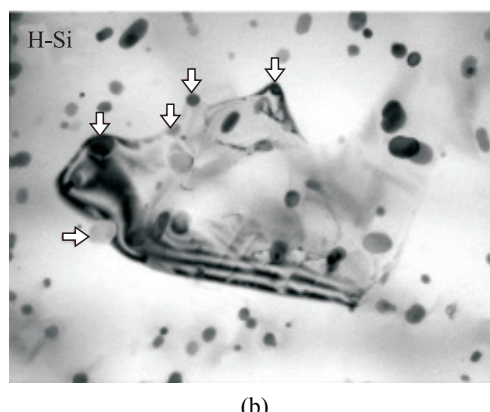
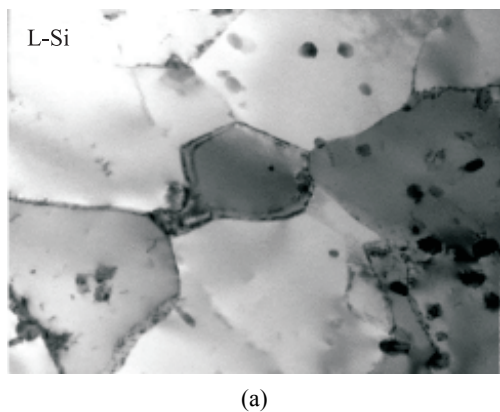


Fig.5. TEM micrographs of Al-Mn-Mg aluminum alloy showing the particle distribution varied with different Si additions, (a) L-Si, and (b) H-Si.

motion. The interaction system between the coherent dispersoids and boundaries must keep the interfacial energy minimization resulting in an extremely low mobility. Thus, the denser the coherent dispersoids precipitate, the greater the ability to retard the recrystallization.

Figure 7(a) shows the influence of the Si contents on the recrystallization texture evolution by isothermal annealing at 340°C for different lengths of time. It can be found that a sharp Cube component has dominated after annealing for 600s. Moreover, the intensities of the residual rolling textures such as components Bs and C turn stronger gradually with increasing the Si concentrations. The orientation densities after fully recrystallization by plotting the intensity from the exact Cube component along Φ towards the Goss component is given in Fig.7(b). It is noted that the evolution of the recrystallization Cube component depends on the Si concentrations. The tendency of texture development

might be ascribed to the particle size distribution as shown in Fig.8. From the literature⁽³⁻⁹⁾, the particle density capable of stimulating nucleation of recrystallization has been considered to be the essential factor for the texture evolution. Being as a potential nucleation site for PSN, therefore, a particle size must exceed a critical diameter d_c to overcome the Gibbs-Thompson effect⁽¹⁶⁾, as Eq.(2)

$$d_c \geq \frac{4l\gamma_{gb}}{3\gamma_{sb} - 2lZ} \dots\dots\dots(2)$$

Where l is the subgrain size, γ_{gb} and γ_{sb} are interfacial energies of the grain boundaries and subgrain boundaries respectively. According to the Shockley-Read equation, the grain boundary ratio $\gamma_{sb}/\gamma_{gb}=0.3$ was used for estimation in this study^(4,8,17). Consequently, the critical particle diameter d_c could be determined.

The number of particles with a diameter larger

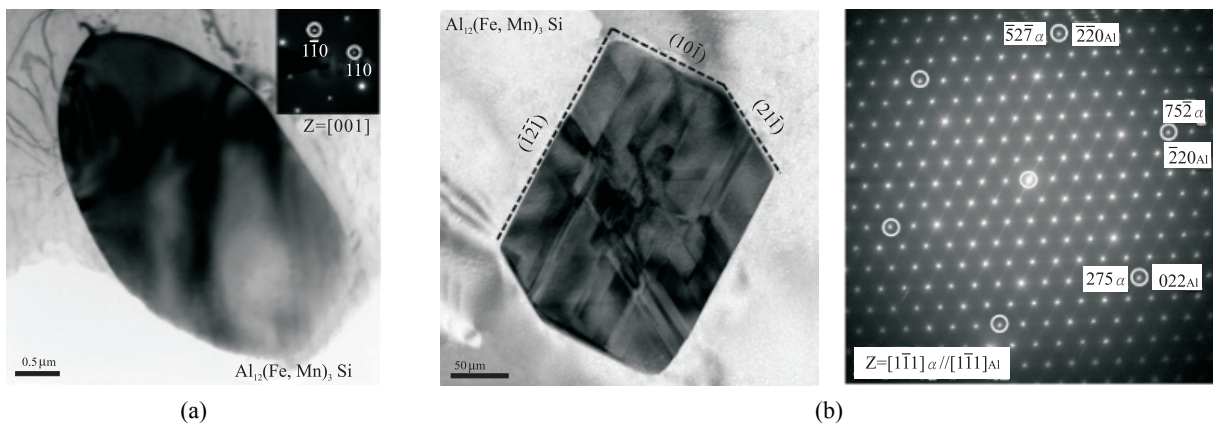


Fig.6. (a) TEM analysis of the α_c dispersoid particles shows high coherency with matrix along $[111]_{Al}$ zone axis. (b) The spheroidized α_c constituent particles.

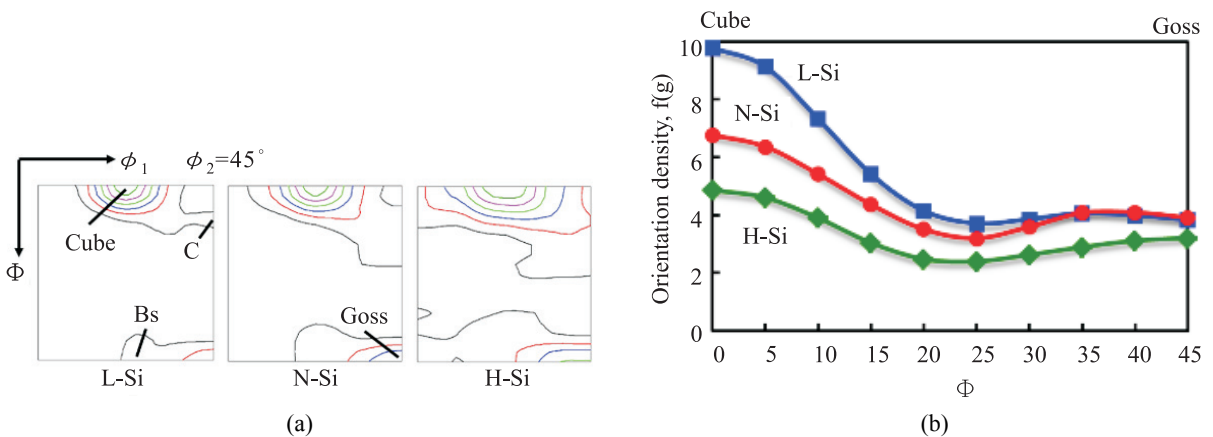


Fig.7. (a) The influence of different Si additions on the recrystallization texture evolution. (b) the intensity from the exact Cube component along Φ towards the G component of the specimens after fully recrystallization.

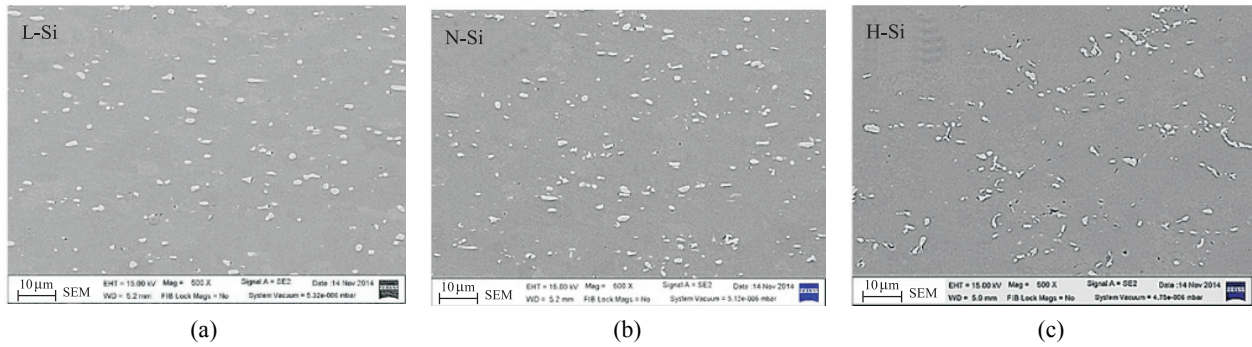


Fig.8. SEM micrographs showing the particle distributions of as-PSCed specimens before annealing: (a) L-Si, (b) N-Si, and (c) H-Si.

Table 3 Influence of the number of particles with diameter larger than d_c on the intensity of Cube component

Sample	L-Si	N-Si	H-Si
l	0.58	0.59	0.59
d_c	3.4	3.4	3.5
No. particles > $d_c/\mu\text{m}^2$	108	198	161
Cube component intensity, f(g)	9.79	6.76	4.86

than d_c was measured as given in Table 3. It is associated with the number of “active” particles for stimulating non-Cube oriented recrystallized grains. That is, a random texture with a low Cube intensity results from a high density of active particles. The Si addition affects the frequency of coarse particles directly. As a consequence, the intensity of the random texture exhibits an evidently dependence on the number of particles with a diameter larger than d_c . It is worthy of note that the number of dispersoids with a diameter larger than d_c of the specimen H-Si was fewer than that of specimen N-Si, however, resulting in the weakest Cube intensity. It might be attributed that the recrystallization development of the specimen H-Si was unfinished due to the extreme pinning force. Hence, it appears to imply that a weakening drag force on grain boundary has a benefit to the development of the Cube orientated nuclei upon the recrystallization period.

4. CONCLUSIONS

1. Various Si additions have a great influence on the recrystallization behavior of the PSCed specimens during annealing. The recrystallized grain growth rate is decelerated with increasing Si contents. That could be ascribed to a larger quantity of the coherent dispersoids precipitated results in strengthening the retarding force on grain/subgrain boundaries upon growth.
2. Evolution of recrystallization texture for PSCed

specimens during annealing shows a strong dependence on the Si additions, i.e. the intensity of Cube component increases with reducing the Si content.

3. Evolution of the recrystallized texture in Al-Mn-Mg aluminum alloy with a bimodal particle distribution could be interpreted quantitatively based on the criterion recommended by Humphreys, excepting the specimen H-Si.
4. Effect of the Si atom solid solution seems to have little influence on the retarding force of the boundary migration.

REFERENCES

1. G. Gaustada, E. Olivetti and R. Kirchainb, Resources, Conservation and Recycling, Jan. 2012, Vol. 58, pp. 79-87.
2. H. D. Merchant, E. J. Westerman and J. G. Morris, Aluminum Alloys for Packaging, TMS, Feb. 1993, pp. 1-16.
3. H. D. Merchant, J. Crane and E. H. Chia, Homogenization and Annealing of Aluminum and Copper Alloys, The Metallurgical Society, Inc., 1988.
4. W.B. Hutchinson, A. Oscarsson and Å. Karlsson, Mat. Sci. Tech., 1989, Vol.5, pp. 1118-1127.
5. W.B. Hutchinson and H.-E. Ekström, Mat. Sci. Tech., 1990, Vol.6, pp. 1103-1111.
6. G. J. Marshall, Mat. Sci. Forum, 1996, Vol. 217-222,

- pp. 19-30.
7. R.K. Bolingbroke and G.J. Marshall, *Mat. Sci. Forum*, 1993, Vol. 113-115, pp. 685-690.
 8. E. H. Chia and H.J. McQueen, *Microstructural Control in Aluminum Alloys: Deformation, Recovery and Recrystallization*, AIME, 1985.
 9. F.J. Humphreys and M. Hatherly, *Recrystalliation and Related Annealing Phenomena*, Pergamon, 1995.
 10. H. M. Chan and F. J. Humphreys, *Acta Metal.*, 1984, Vol. 32, No. 2, pp. 235-243.
 11. F.J. Humphreys, *Acta Metall.*, 1977, Vol. 25, pp. 1323-1344.
 12. T. Pettersen¹, Y. Li, T. Furu¹ and K.Marthinsen, *Mat. Sci. Forum*, 2007, Vol. 558-559, pp. 301-306.
 13. Chung-Yi Yu, *China Steel Report*, PJ01679.
 14. V. Randle and O. Engler, *Introduction to Texture Analysis: Macrostructure, Microstructure and Orientation Mapping*, CRC Press, 2000.
 15. R. D. Doherty, *Metal Science*, 1982, Vol. 16, issue 1, pp. 1-14.
 16. D. A. Portor and K. E. Easterling, *Phase Transformations in Metals and Alloys*, second edition, Chapman & Hall, 1992.
 17. S. Benum and E. Nes, *Acta Metal.*, 1997, Vol. 45, No. 11, pp. 4593-4602. □